*J. Fluid Mech.* (2009), *vol.* 635, *pp.* 245–273.  
doi:10.1017/S0022112009007563

# Intrusive gravity currents from finite-length locks in a uniformly stratified fluid

J. R. MUNROE[1], C. VOEGELI[2], B. R. SUTHERLAND[3]†, V. BIRMAN[4] AND E. H. MEIBURG[4]

[1]Department of Physics, University of Alberta, Edmonton, AB, Canada T6G 2G7

[2]Department of Mathematical and Statistical Sciences, University of Alberta, Edmonton, AB, Canada T6G 2G1

[3]Departments of Physics and Earth and Atmospheric Sciences, University of Alberta, Edmonton, AB, Canada T6G 2G7

[4]Department of Mechanical Engineering, University of California, Santa Barbara, CA 93106, USA

(Received 29 January 2007; revised 8 April 2009; accepted 8 April 2009)

Gravity currents intruding into a uniformly stratified ambient are examined in a series of finite-volume full-depth lock-release laboratory experiments and in numerical simulations. Previous studies have focused on gravity currents which are denser than fluid at the bottom of the ambient or on symmetric cases in which the intrusion is the average of the ambient density. Here, we vary the density of the intrusion between these two extremes. After an initial adjustment, the intrusions and the internal waves they generate travel at a constant speed. For small departures from symmetry, the intrusion speed depends weakly upon density relative to the ambient fluid density. However, the internal wave speed approximately doubles as the waves change from having a mode-2 structure when generated by symmetric intrusions to having a mode-1 structure when generated by intrusions propagating near the bottom. In the latter circumstance, the interactions between the intrusion and internal waves reflected from the lock-end of the tank are sufficiently strong and so the intrusion stops propagating before reaching the end of the tank. These observations are corroborated by the analysis of two-dimensional numerical simulations of the experimental conditions. These reveal a significant transfer of available potential energy to the ambient in asymmetric circumstances.

## 1. Introduction

Gravity currents are flows driven by horizontal density variations. In the simplest arrangement, heavy fluid flows beneath a uniform ambient. This describes a bottom-propagating gravity current and models natural examples such as sea breezes or cold thunderstorm outflows. At sufficiently large spatial and slow temporal scales a gravity current may be affected by a continuously stratified ambient and, in particular, may generate internal gravity waves. An internal gravity wave is caused by the displacement of a fluid parcel from rest which responds to a restoring force due to buoyancy. This interaction can be more substantial if the density of the gravity current matches the density of the stratified ambient at some vertical level, in which case it is referred to as an intrusion. Such a circumstance may arise, for example, at the outflow of a

† Email address for correspondence: bruce.sutherland@ualberta.ca

thunderstorm near the tropopause or when a rising plume spreads horizontally where it encounters an atmospheric inversion (see Simpson 1997 for a comprehensive review of examples of gravity currents in environmental and industrial contexts.)

In laboratory experiments the most commonly studied gravity current is heavy fluid propagating along a rigid bottom boundary beneath a uniform ambient (Keulegan 1957; Benjamin 1968; Simpson 1972; Britter & Simpson 1978; Simpson & Britter 1979; Huppert & Simpson 1980; Klemp, Rotunno & Skamarock 1994; Shin, Dalziel & Linden 2004). In a typical lock-release experiment in a long rectangular tank, a finite volume of uniform-density salt water is held behind a gate in a lock. On the other side of the gate is uniform ambient fluid. When the gate is removed, horizontal density differences establish a horizontal pressure gradient which causes the current to flow into the ambient and the ambient to move backward into the lock as a return flow. Observations show that the speed of the gravity current is constant for several lock lengths. A prediction of this speed was given by the analytical theory of Benjamin (1968) which examined the prototype problem of the gravity current of a heavy fluid of density $\rho_c$ propagating beneath lighter fluid of density $\rho_a$. For a steady current, the front speed $U$ is given by

$$U = Fr_B\sqrt{g'H}, \tag{1.1}$$

where $g' = g(\rho_c - \rho_a)/\rho_a$ is the reduced gravity, $H$ is the total depth of the fluid and $Fr_B$ is the Froude number. Using mass and momentum conservation within a control volume, Benjamin (1968) determined that

$$Fr_B(\tilde{h}) = \sqrt{\frac{\tilde{h}(1-\tilde{h})(2-\tilde{h})}{1+\tilde{h}}}, \tag{1.2}$$

in which $\tilde{h} = h/H$ is the relative depth of the current head. In particular, for an energy-conserving current released from a full-depth lock, $h = H/2$ and $Fr_B = 1/2$.

Bottom-propagating gravity currents beneath a two-layer ambient were examined by Rottman & Simpson (1983), and the first experiments and simulations of a gravity current travelling along a rigid bottom under a continuously stratified fluid were performed by Maxworthy *et al.* (2002). The latter found an empirical relationship between the speed of the front of the gravity current and the parameters of the system such as the density of the current and the strength of the stratification. By analogy with (1.1) they found

$$U = FrNH, \tag{1.3}$$

in which $N$ is the buoyancy frequency, which characterized the stratification of the ambient, and $Fr$ is the Froude number appropriate for gravity currents in a stratified ambient. For gravity currents having the same density as that at the base of the ambient, they found $Fr \simeq 0.266$. They also determined that the aspect ratio of the lock is unimportant as far as the initial dynamics of the gravity current were concerned. They were interested in the transition from the supercritical case to the subcritical case. In the supercritical case the current travelled faster than the fastest long-wave speed and no internal waves were generated. In the subcritical case, internal waves were generated and these were observed to act back upon the gravity current causing it to advance in a pulsating fashion.

Using an extension of shallow water theory from homogeneous to stratified ambients, Ungarish & Huppert (2002) showed that their model well captured the initial slumping phase of such bottom propagating gravity currents observed both in

fully nonlinear numerical simulations and in experiments. Specifically, the speed was predicted by (1.3) with

$$Fr = Fr_B(\tilde{h})(1 - S + S\tilde{h}/2)^{1/2}, \tag{1.4}$$

in which $S = (\rho_b - \rho_0)/(\rho_\ell - \rho_0)$ is the ratio of the density difference between the bottom and top of the ambient to the density difference between the lock fluid and the top of the ambient. The prediction was developed for bottom-propagating gravity currents, in which case $0 \leqslant S \leqslant 1$ (Ungarish 2006). For a full-depth lock-release current, one expects $\tilde{h} = 1/2$ in which case $Fr_B = 1/2$, as above. If the lock fluid density matches that at the bottom of the ambient, $S = 1$ and so $Fr = Fr_0 \equiv 1/4$. This result lies in close agreement with the experimental observation of Maxworthy *et al.* (2002).

More recently Ungarish (2006) derived an analytic model based upon shallow water theory that predicted the long-time evolution of bottom-propagating gravity currents. These results were compared with numerical simulations (Birman, Meiburg & Ungarish 2007) and showed good agreement for shallow-depth currents ($\tilde{h} \ll 1/2$) in relatively weakly stratified fluids. For subcritical currents in strong stratification the theory predicted multiple solutions for the current speed and the simulations showed the current speed matched better with solutions slower than the fastest predicted speed.

The evolution of intrusions is less understood than that of gravity currents (Holyer & Huppert 1980; Britter & Simpson 1981; Lowe, Linden & Rottman 2002; Sutherland, Kyba & Flynn 2004; Monaghan 2007). By allowing the interface ahead of an intrusion to be vertically displaced, Benjamin's (1968) theory was adapted to predict the propagation speed of intrusions in a two-layer fluid (Flynn & Linden 2006). This speed was predicted on heuristic grounds by Cheong, Kuenen & Linden (2006), who estimated the speed by relating the available potential energy of the system before the lock fluid was released to the consequent kinetic energy of the intrusion.

Numerous experiments have been performed that examine the speed and structure of intrusions propagating at mid-depth in uniformly stratified ambient, these resulting either from a full-depth lock-release (Sutherland & Nault 2007) or from a localized mixed patch ( Wu 1969; Schooley & Hughes 1972; Manins 1976; Amen & Maxworthy 1980; Silva & Fernando 1998; Sutherland, Chow & Pittman 2007).

Only recently have laboratory experiments been performed to examine the asymmetric circumstance of intrusions propagating at arbitrary depth in a uniformly stratified fluid (Bolster, Hang & Linden 2008). These authors extended the Cheong *et al.* (2006) result by fitting a quadratic to the mid-depth, top and bottom propagating intrusion speeds, that were predicted by (1.3) with $Fr_0 = 1/4$ (Ungarish & Huppert 2002; Ungarish 2006) and $Fr_0 = 0.266$ (Maxworthy *et al.* 2002). Thus they heuristically predicted that the speed of an intrusion propagating at depth $h_L$ is given by (1.3) with

$$Fr = Fr_0\sqrt{3\left(\frac{h_L}{H} - \frac{1}{2}\right)^2 + \frac{1}{4}}. \tag{1.5}$$

They found good agreement with both numerical simulations and laboratory experiments, the theory more closely matching the experimental results using $Fr_0 = 1/4$.

Whereas Bolster *et al.* (2008) examined the initial intrusion speed, this paper focuses upon the generation of internal waves by asymmetric intrusions and studies the consequent influence of internal waves upon the long-time evolution of the intrusion. The length of the lock is small compared with the full length of the tank so that the initial behaviour of the intrusions as well as the long-time behaviour, which is affected by the motion of internal waves in the ambient, can be examined. In these

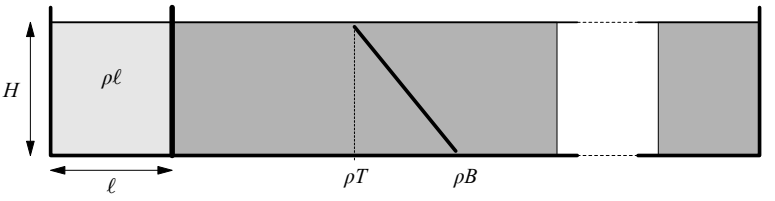


FIGURE 1. Set-up and definition of parameters for intrusion experiments.

experiments intrusions were created by having an intermediate density between the average density of the ambient and the density at the base of the stratification. We also conducted experiments in which the density of the fluid in the lock exceeded that of the bottom of the stratification. As such these investigations bridge the gap between studies of a bottom-propagating current and of a symmetric intrusion in a uniformly stratified ambient.

Shallow-water theory and numerical simulations (Ungarish 2005) have predicted that the intrusion should evolve from a steady-state (constant speed) phase to a decelerating (self-similar) phase. Such behaviour is anticipated by shallow-water theory (Ungarish 2006) because the current speed is predicted to decrease as the current depth decreases according to (1.4). However, our experiments show this is not the case for intrusions released from a full-depth lock. Consistent with Sutherland & Nault (2007), symmetric intrusions are found to propagate at constant speed up to 20 lock lengths with no appearance of a self-similar phase. This occurs despite the fact that the head height continuously decreases with distance from the lock. Such behaviour occurred because the intrusion evolved into the form of a closed-core solitary wave. For asymmetric intrusions, the return flow launches internal waves that reflect off the lock-end of the tank and then catch up with the intrusion head, halting its advance. Until this occurs the intrusion propagates as constant speed even as the waves act to reduce the head depth to zero. Internal waves thus play an important role in the long-time evolution of intrusions as we show quantitatively through an analysis of the wave properties both in experiments and in numerical simulations.

The paper is organized as follows. The experimental set-up and analysis methods are described in § 2 and the experimental results are presented in § 3. The analyses focus upon the intrusion speed and the impact of internal gravity waves generated by the intrusion and upon how the waves can cause the intrusion to stop before reaching the end of the tank. The details of the numerical simulations are in § 4. Conclusions and future work are given in § 5.

## 2. Experimental set-up and analysis

Experiments were performed in a glass tank measuring $L = 197.1$ cm long $\times$ 17.4 cm wide $\times$ 48.5 cm tall as shown in figure 1. The tank was left open to the atmosphere at the top. Salt water with a linearly stratified density profile filled the tank using the standard 'double bucket' technique (Oster 1965). Dye lines of red food colouring were added every 5 cm while the tank was being filled in order to visualize internal gravity waves generated in the experiment. The total depth $H$ of the ambient was either 30 cm or 15 cm for all experiments. The strength of the stratification, measured by the buoyancy frequency

$$N = \sqrt{-\frac{g}{\rho_0}\frac{\mathrm{d}\rho}{\mathrm{d}z}}, \tag{2.1}$$

varied between 0.34 and 2.0 $s^{-1}$ (bottom to top density differences between 0.003 and 0.14 g $cm^{-3}$) for different experimental runs. A vertically traversing 50 cm long Fast Conductivity and Temperature Probe (Precision Measurement Engineering Corlsbod, CA, USA) was used to measure the density profile of the stratification. The probe was recalibrated before each experiment.

The experiments had corresponding Reynolds numbers, based upon $N$ and $H$, ranging from $Re(=NH^2/\nu) \simeq 8 \times 10^3$ to $1.8 \times 10^5$. These values were sufficiently large and so the viscosity was not expected to play a significant role in the dynamics of the intrusions. The Schmidt number was $Sc = 10^3$.

After filling the tank, a 0.4 cm thick gate was inserted between a pair of vertical glass guides to create a water-tight lock at one end of the tank. The length of the lock was set to $\ell = 8.5$, 18.5 or 38.5 cm. Most of the experiments were performed with a lock length of $\ell = 18.5$ cm.

A small amount of blue dye was added to the fluid in the lock and the contents were vigorously stirred until the lock fluid had uniform density. The dye allowed the intrusion to be visualized during the experiment and was introduced in sufficiently low concentrations that it did not significantly change the density of the fluid in the lock.

In some experiments, additional salt was added to the lock fluid before its contents were mixed. After mixing, the density of the lock was measured using a hydrometer placed in the lock. In some experiments, the density was measured using an Anton Paar density meter.

The intrusion propagated at a depth such that the density of the lock fluid was equal to the density of the undisturbed stratified fluid at that depth. If no salt was added, the lock-fluid density $\rho_\ell$ was the average $\bar{\rho}$ of the density at the top $\rho_T$ and the density at the bottom $\rho_B$ of the ambient and the intrusion travelled at mid-depth, $h/H = 1/2$. Here $h$ is the vertical position of the intrusion measured from the bottom of the tank and $H$ is the total depth of the ambient. Adding salt to the lock increased the density of the lock fluid. If $\bar{\rho} < \rho_\ell < \rho_B$, the intrusion propagated between the bottom and mid-depth. Since the stratification was linear, we can calculate this intrusion depth to be $h/H = (\rho_B - \rho_\ell)/(\rho_B - \rho_T)$. Analogous to Sutherland *et al.* (2004), the depth can be characterized by a non-dimensional parameter

$$\epsilon = \frac{\rho_\ell - \bar{\rho}}{\rho_B - \rho_T}. \tag{2.2}$$

Note that $h/H = 1/2 - \epsilon$, so both $h/H$ and $\epsilon$ are measures of the relative density of the lock-fluid subject to $0 < h/H < 1$ and $-1/2 < \epsilon < 1/2$ for $\rho_T < \rho_\ell < \rho_B$. If $\rho_\ell \geqslant \rho_B$ then the intrusion runs along the bottom of the tank and $\epsilon > 1/2$ even though $h/H = 0$. Although we did not run any experiment where $\rho_\ell < \bar{\rho}$ (which correspond to $\epsilon < 0$ or $h/H > 1/2$) we assume the experiment is symmetrical about $\epsilon = 0$ since the problem is Boussinesq. When $\epsilon > 1/2$ the gravity current runs along the bottom and when $\epsilon < -1/2$ the gravity current runs along the surface. The choice of a non-dimensional parameter for density is not unique. For example, in Maxworthy *et al.* (2002) the relative density was represented by $R = (\rho_\ell - \rho_T)/(\rho_B - \rho_T)$. We have chosen to use $\epsilon$ because it serves to emphasize the symmetry of the problem.

A digital video camera (3 CCD Sony DVD Steadycam) was positioned 3.5 m from the front of the tank so that the whole length of the tank was in the camera's field of view. Each experiment was recorded onto video tape for later analysis. The frame rate was as small as $\Delta t = 1/30$ s and the spatial resolution allowed disturbances as small as $\Delta z \simeq \Delta x \simeq 0.4$ cm to be visualized. The dynamics of the system were primarily

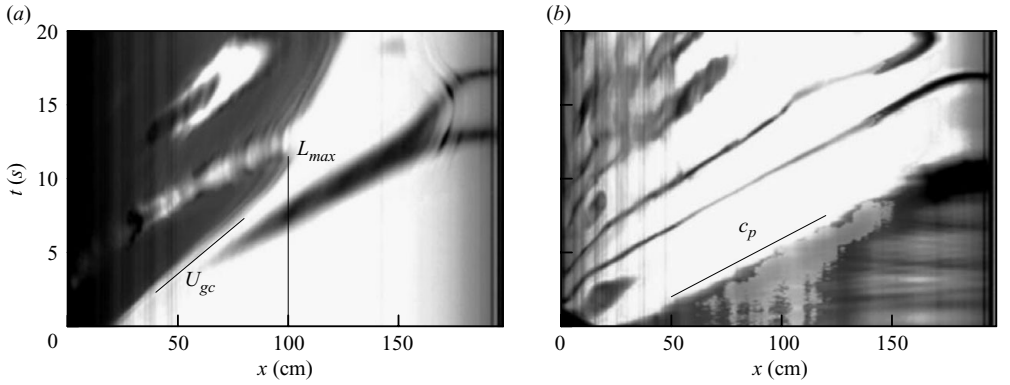


FIGURE 2. (*a*) Horizontal time series taken from experiments with $\epsilon = 0.27$, $H = 30\,\text{cm}$, $N = 1.8\,\text{s}^{-1}$ and $\ell = 18.5\,\text{cm}$. The time series is taken from a horizontal slice through movies of the experiment situated $z = 7.5\,\text{cm}$ above the bottom of the tank close to the neutral buoyancy level of the lock fluid. The superimposed solid lines show the intrusion speed $U_{gc}$ and propagation distance $L_{max}$. The sloped dark wedge ahead of the intrusion results from the vertical displacement of a dye line through the level $z = 7.5\,\text{cm}$. The displacement occurs due to internal waves launched ahead of the intrusion. (*b*) Horizontal time series taken from the same experiment at the $z = 25\,\text{cm}$. The superimposed solid line indicates the phase speed of internal waves moving ahead of the intrusion. The slope dark lines occurring at later times result from the dye line at $z \simeq 25\,\text{cm}$ moving vertically through the plane $z = 25\,\text{cm}$ above and behind the intrusion head.

two-dimensional, as corroborated by the numerical simulations discussed later. Thus we did not analyse the cross-tank structure of the gravity current as it evolved.

After the tank was set up, the gate was quickly removed. An unavoidable side effect of this procedure was to introduce turbulence (and hence mixing) as fluid is dragged along by the upward movement of the gate. As is typical in lock-release experiments (Simpson 1982), this mixing did not significantly affect the evolution of the intrusion after propagating a small distance from the lock.

After the removal of the gate, the lock fluid collapsed into an intrusive gravity current which propagated horizontally along the length of the tank. The centre of the current was at a neutrally buoyant depth. We marked the end of the experiment as the point in time at which the far endwall effects, such as the reflection of waves, started to impact the evolution of the intrusion.

The 'DigImage' software package (Dalziel 1992) was used to perform most of the analyses. One of the features of DigImage was to create horizontal and vertical time series from the raw video signal recorded during the experiment. A horizontal time series was constructed by choosing a vertical position (a particular pixel coordinate), extracting a row of pixels at that height from successive frames of the video and vertically stacking these horizontal slices. Vertical time series were created in a similar manner from successive vertical slices.

To measure the position of the gravity current as a function of time, we used a horizontal time series taken at a vertical position corresponding to the depth of the intrusion. The front of the intrusion was identified in the horizontal time series by the diagonal contour separating the darkly dyed intruding lock fluid and the relatively light intensity ambient. This is shown, for example, in figure 2(*a*). The horizontal time series was taken at the horizontal level corresponding to the neutral buoyancy level of the lock fluid. After a brief acceleration time, the intrusion propagated at a nearly constant speed, $U_{gc}$. The distance over which the intrusion propagated in

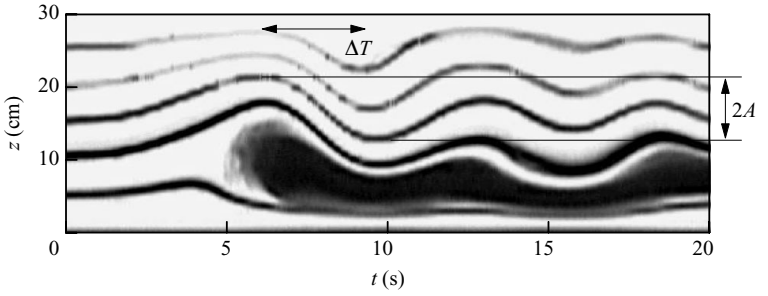


FIGURE 3. Vertical time series from experiment with $\epsilon = 0.27$ taken at $x = 60$ cm showing the measurement of the half-period $\Delta T$ of the leading internal wave and the measurement of the peak-to-peak displacement $2A$ of a dye line.

steady state depended upon the consequent interaction between the intrusion and internal waves. In all experiments, the speed was found to be constant between one lock length and at least three lock lengths from the gate. The velocity of the intrusion head was thus determined by finding the slope of the line, typically between one and three lock lengths from the gate, as indicated in figure 2(*a*). As was characteristic of all experiments, the intrusion travelled at an initial constant speed at least up to three lock lengths. We denote the horizontal distance travelled by the intrusion before the nose velocity first became zero as the propagation distance $L_{max}$ which is also indicated in figure 2(*a*). The notation $L_{max}$ is not meant to indicate that the intrusion goes no further than this distance. At later times the intrusion moves forward in a pulsating way but, as we will show, this is a consequence of internal waves advecting the lock fluid as was observed by Maxworthy *et al.* (2002). The motion does not result from horizontal density gradients establishing horizontal pressure gradients, which is the mechanism usually ascribed to drive a gravity current.

The dye lines added when the tank was being filled allow for the analysis of internal waves generated by the intrusion. In most experiments we measured the wave phase speed $c_p$ of the first wave generated by creating a horizontal time series at the $z = 25$ cm dye line from the bottom of the tank (e.g. figure 2*b*). The superimposed vertically offset lines indicate slopes used to measure speeds. Because the intrusions propagated at mid-depth or below, a horizontal time series at this height revealed a clear signal of the dye line being displaced by the waves without contamination by the intrusion itself. The slope of the contour in the horizontal time series marking the initial displacement of the dye line allowed us to compute the phase speed.

The frequency of the waves was found by using a vertical time series at $x = 60$ cm from the lock-end of the tank, as shown in figure 3. We measured the time $\Delta T$ between the first crest and first trough to pass this point. We estimated the period to be $T = 2\Delta T$ and the frequency to be $\omega = 2\pi/T$.

The internal wave amplitude was found by measuring the maximum displacement of each dye line and dividing by two as shown for the third dye line in figure 3. These amplitude measurements were performed using vertical time series at $x = 60$ cm and $x = 160$ cm from the lock-end of the tank.

## 3. Experimental results

Figures 4–6 show three experiments demonstrating the characteristic behaviour of symmetric ($h/H = 1/2$), asymmetric ($0 < h/H < 1/2$) and bottom-propagating

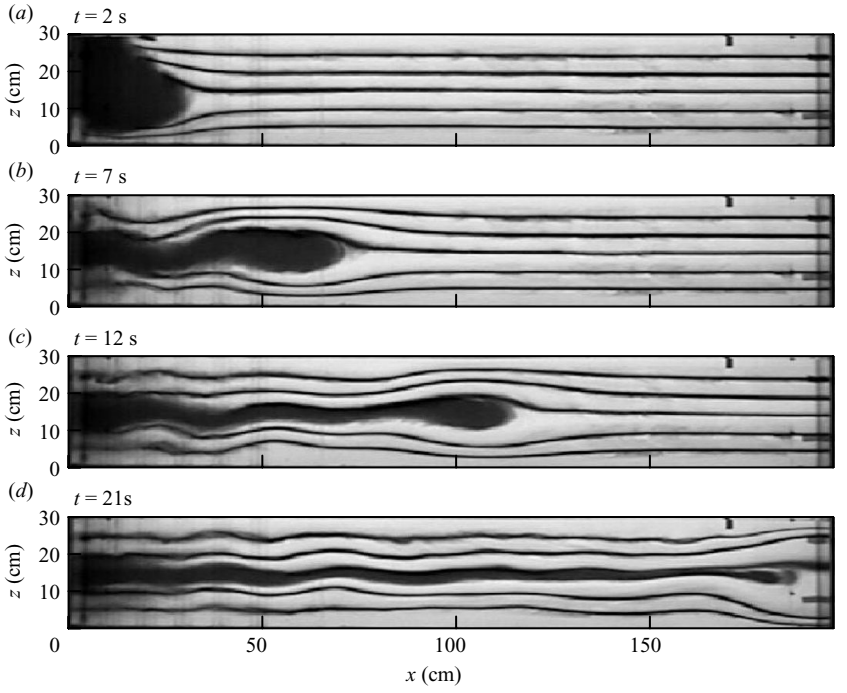


FIGURE 4. Snapshots from experiment with $\epsilon = 0$, for which the intrusion travels along the middle of the tank, at times (*a*) $t = 2$ s ($Nt \simeq 2$), (*b*) $t = 7$ s ($Nt \simeq 14$), (*c*) $t = 12$ s ($Nt \simeq 20$) and (*d*) $t = 21$ s ($Nt \simeq 42$).

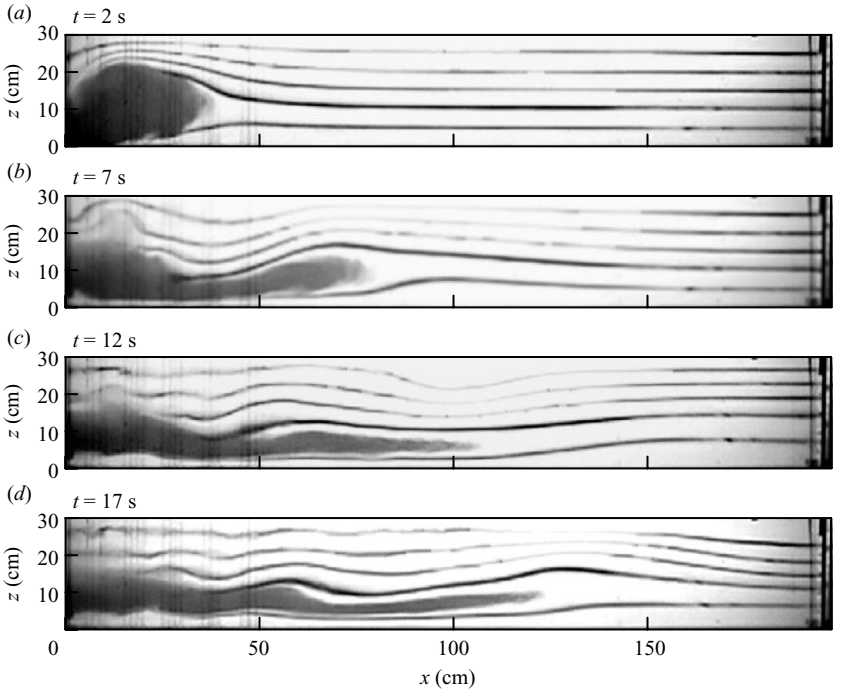


FIGURE 5. Snapshots from experiment with $\epsilon = 0.27$, for which the intrusion travels along the middle of the tank, at times (*a*) $t = 2$ s ($Nt \simeq 3.4$), (*b*) $t = 7$ s ($Nt \simeq 11.8$), (*c*) $t = 12$ s ($Nt \simeq 20.2$) and (*d*) $t = 17$ s ($Nt \simeq 28.7$). Corresponding horizontal and vertical time series are shown in figures 2 and 3, respectively.

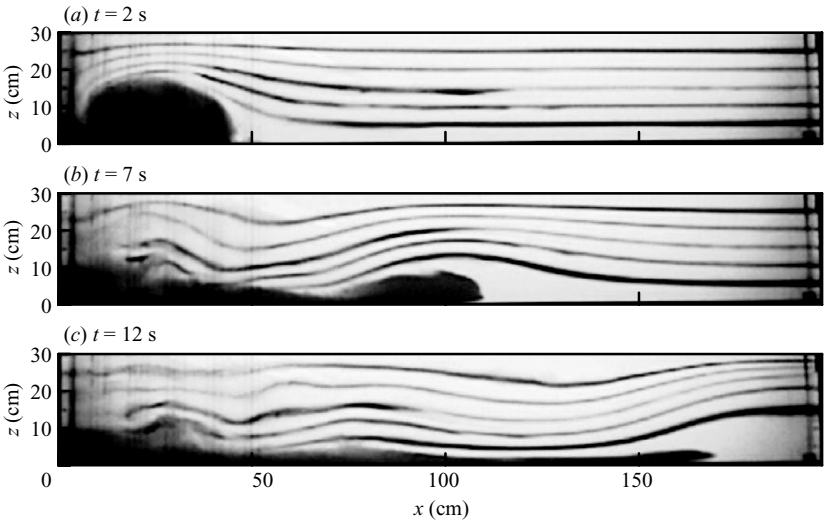


FIGURE 6. Snapshots from experiment with $\epsilon = 0.54$, for which the intrusion travels along the middle of the tank, at times (*a*) $t = 2$ s ($Nt \simeq 3.6$), (*b*) $t = 7$ s ($Nt \simeq 12.6$) and (*c*) $t = 12$ s ($Nt \simeq 21.6$).

($h/H = 0$) intrusions. For these experiments, the depth of the tank was $H = 30$ cm, the lock length was $\ell = 18.5$ cm and the buoyancy frequency ranged from $N = 1.7$ to $2.0\,\mathrm{s}^{-1}$.

For the experiment shown in figure 4, no salt was added to the lock so that $\epsilon = 0$. In this case the intrusion travelled down the middle of the tank. In the initial collapse stage at $t = 2$ s (figure 4*a*) the lock fluid intrudes into the ambient and a return flow above and below the intrusion moves into the lock. The asymmetry in the return flow occurs because the gate is not removed instantaneously. At $t = 7$ s (figure 4*b*) a clear head develops which travels at a constant speed along the tank with a sinuous tail in its lee. At $t = 21$ s (figure 4*d*) the intrusion head has thinned considerably and the intrusion reaches the end of the tank. The leading internal wave is locked to the head of the intrusion and dye lines are displaced only slightly in front of the head. The dye lines reveal the existence of a mode-2 internal wave, for which dye lines displace upward in the top half and downward in the bottom half of the tank.

In figure 5, salt was added to the lock so that $\epsilon = 0.27$. Note that the intrusion is asymmetric. In the initial collapse stage at $t = 2$ s (figure 5*a*) the dark lock fluid intrudes into the ambient with return flows occurring above and below. In figure 5(*b*) a clear head develops shortly after being released. The intrusion propagates at a constant speed until $t = 12$ s (figure 5*c*) at which time the intrusion head gradually collapses due to the advance from behind of an internal wave generated by the return flow. The leading wave is far in advance of the head and has reached the end of the tank. After stopping, the lock fluid is effectively incorporated into the wave field. In the image shown at 17 s (figure 5*d*) the dyed fluid has been carried a short distance forward of the original stopping distance through the action of the waves. The motion of the front of the intrusion head over time is more clearly shown through the horizontal time series in figure 2(*a*).

In figure 6, salt was added to the lock so that $\epsilon = 0.54$. The current travelled along the bottom of the tank. In the initial collapse stage at $t = 2$ s (figure 6*a*) lock fluid flows beneath the ambient fluid. The ambient fluid flows above the lock fluid into the

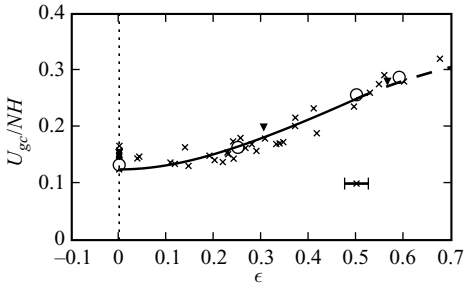


FIGURE 7. Relative intrusion speed plotted against $\epsilon$ as measured in experiments with $\ell = 18.6\,\text{cm}$ and $H = 30\,\text{cm}$ (crosses) and $H = 15\,\text{cm}$ (upside-down triangles). The open circles show the corresponding measurements determined from four numerical simulations. Plotted as a solid line is the predicted speed of intrusions determined by the adaption of Cheong *et al.* (2006) theory (Bolster *et al.* 2008) as given by (3.1). The dashed line shows the prediction of shallow-water theory for bottom-propagating gravity currents as given by (3.2). Typical errors in the estimate of $\epsilon$ are shown towards the lower right-hand corner of the plot.

lock. At $t = 7\,\text{s}$ (figure 6*b*) the current with a clearly defined head is propagating at a constant speed. There is a small wedge of undyed fluid beneath the head. Since the lock fluid was slightly denser than the bottom density of the ambient there must have been some entrainment of ambient fluid to lower the density of the head, for example, through interactions with the viscous bottom boundary layer (Härtel, Meiburg & Necker 2000). At $t = 12\,\text{s}$ (figure 6*c*) the head is a thin wedge shape and the leading wave has reached the end of the tank. The dye lines indicate a mode-1 internal wave for which all the dye lines are displaced upwards above the current head.

In experiments with still larger $\epsilon \gtrsim 0.65$ (not shown) the gravity current excites mode-1 waves but the current is observed to propagate nearly to the end of the tank before its speed is affected by interactions with the wave reflecting from the endwall of the tank.

### 3.1. *Intrusion speed*

In all our experiments, after a brief acceleration time the gravity current propagated at a constant speed for a distance along the tank. Figure 7 shows the initial intrusion speed as a function of the relative density of the lock fluid. The error bars on $\epsilon$ indicate the sensitivity in determining this parameter from traverse data. The appropriate characteristic scaling of the intrusion speed is given by $NH$ in which $N$ is given by (2.1). The minimum intrusion speed occurs when $\epsilon = 0$, which corresponds to the density of the lock fluid being equal to the average density of the ambient. As $\epsilon$ moves away from zero, the speed of the intrusion increases although its speed does not change much for $0 \leqslant \epsilon \lesssim 0.2$. As the system makes the transition from an intrusion to a bottom-propagating current the speed increases significantly with $\epsilon$.

These intrusion results are compared with the prediction of Bolster *et al.* (2008) (1.5), which is recast in terms of the $\epsilon$ parameter to give

$$\frac{U_{gc}}{NH} = Fr_0\sqrt{3\epsilon^2 + 1/4}, \tag{3.1}$$

in which we use $Fr_0 = 0.25$, as predicted by Ungarish (2006). The curve is plotted as the solid line in figure 7. Consistent with Bolster *et al.* (2008) (who also examined $-0.5 < \epsilon < 0$ cases), we find the theory agrees well with the observed speeds.

The good fit might be expected because (3.1) results from making a quadratic fit to the square of the velocity as a function of $\epsilon$ insisting only that the speed in the case

$\epsilon = 1/2$ is set by $Fr_0 = 1/4$. By symmetry, the speed in the case $\epsilon = 0$ should be half this value and the change in speed as a function of $\epsilon$ should be zero about $\epsilon = 0$. One could also form a good quadratic fit by requiring the speed, not the square of the speed, be quadratic. However, Bolster *et al.* (2008) argue that fitting the square of the speed is appropriate on energetic grounds. The available potential energy stored in the lock is released both to the motion of the intrusion and the kinetic and available potential energies of the ambient. Assuming the partition of energy into the intrusion and ambient are in proportion, it is appropriate to compare the kinetic energy of the intrusion, proportional to its velocity squared, to the available potential energy of the lock fluid.

The speed of bottom-propagating currents (for which $\epsilon > 1/2$) is influenced not only by the available potential energy of the lock fluid but also by the normal force of the bottom of the tank acting upon the current. Such effects were accounted for by Ungarish (2006), who used Long's model (1953, 1955) and shallow-water theory to extended Benjamin's theory (1968) to gravity currents in stratified environments. Recasting (1.4) in terms of $\epsilon$ and using $\tilde{h} = 1/2$, appropriate for a full-depth lock release, the speed is predicted to be

$$\frac{U_{gc}}{NH} = Fr_0 \sqrt{\frac{4\epsilon - 1}{\epsilon + 1/2}}. \tag{3.2}$$

Here we have related $S$ to $\epsilon$ using $S = 1/(|\epsilon| + 1/2)$. This curve is plotted as the dashed line in figure 7 for $\epsilon \geqslant 1/2$.

We find that the theory does reasonably well though it moderately underpredicts the speed of currents with $\epsilon \simeq 0.7$. This could be a consequence of experimental error, however a similar discrepancy between numerical simulations and shallow-water theory for full-depth lock-release currents was noted by Birman *et al.* (2007). Nonetheless, the agreement is promising considering that the full-depth lock-release case is an extreme extension of shallow-water theory: predicting the current speed is 'problematic' because of the strong return flow in the ambient above the intrusion (Ungarish 2006).

The agreement may lead one to conclude that the excitation of internal waves is inconsequential in establishing the steady-state speed. However, the situation is more 'subtle' than this (Bolster *et al.* 2008). The very process of collapse means that the stratified ambient must be displaced above and below the head of the intrusion, a process that extracts part of the available potential energy from the lock fluid and which necessarily excites internal waves if not ahead of the current, certainly in its lee. In part for this reason, but also because the mean ambient density ahead of the intrusion is reduced, the Froude number for a bottom propagating current with $\epsilon = 1/2$ is $Fr_0 \simeq 1/4$ (Ungarish 2006) and not $Fr_0 = 1/2$, as would be the case for a gravity current in a uniform-density ambient (Benjamin 1968).

The discussion so far has focused upon the initial speed of the intrusion and bottom-propagating gravity currents. But the main interest of this paper is upon its consequent evolution. Shallow-water theory predicts that the currents decelerate after propagating one lock length as a consequence of the decreased depth of the current head (e.g. see figure 4 of Ungarish 2006). However, we find this is not the case. Not only does the available potential energy released from the lock go into the kinetic energy of the current, but it is also transformed into the available potential energy and kinetic energy of the ambient. It is the transformation of energy into the latter and the consequent interactions between the ambient and intrusion that result in

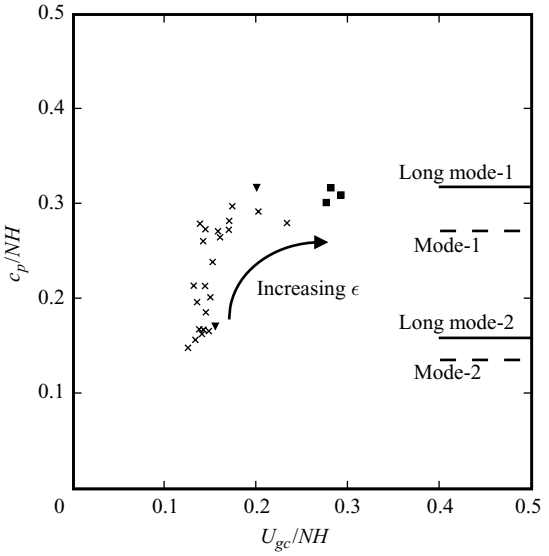


FIGURE 8. Phase speed of the leading internal wave versus intrusion speed. The solid lines give the long-wave speeds of mode-1 and mode-2 waves and the dashed lines give the wave speeds of linear waves of mode-1 and mode-2 with frequency $\omega = 0.52N$. Points are plotted as crosses for $\epsilon \leqslant 0.5$ and $H = 30$ cm, as upside-down triangles for $\epsilon \leqslant 0.5$ and $H = 15$ cm, and as solid squares for $\epsilon > 0.5$.

intrusions propagating long distances from the lock at constant speed even as the intrusion head height decreases. In intermediate $\epsilon$ cases, the ambient can then act abruptly to halt its advance.

Clearly the return flow plays an important role in the generation of internal waves and their consequent impact upon the flow evolution. In § 3.2 we examine the observed characteristics of these waves and so estimate the relative energy associated with wave generation and their consequent impact upon the intrusion head.

### 3.2. *Internal gravity waves*

The release of the lock fluid generated internal waves, which were visualized by the vertical deflection of the horizontal dye lines in the tank. The internal waves were vertically trapped between the rigid bottom of the tank and the free surface. The properties of the internal gravity waves generated in this experiment are set by the geometry of the tank, the stratification of the ambient and the density of the intrusion. The characteristics of the leading internal wave were determined from the initial displacement of the dye lines occurring in advance of the head of the intrusion. It is assumed that the trailing internal waves resulting from the return flow that reflects off the endwall of the lock have the same characteristics as the leading waves. For example, horizontal time series as shown in figure 2 reveal the phase speed of leading wave (indicated by the superimposed line labelled $c_p$) and that of the trailing waves (indicated by the slope of the black dye lines occurring approximately 5 and 10 s later) consistently match.

Figure 8 shows the phase speed $c_p$ plotted against the gravity current speed $U_{gc}$. For $\epsilon = 0$, the waves travel at the same speed as the gravity current and are consistent, for example, with the experiment shown in figure 4. As $\epsilon$ increases from 0, the wave speed increases quickly while the gravity current speed increases slowly, consistent

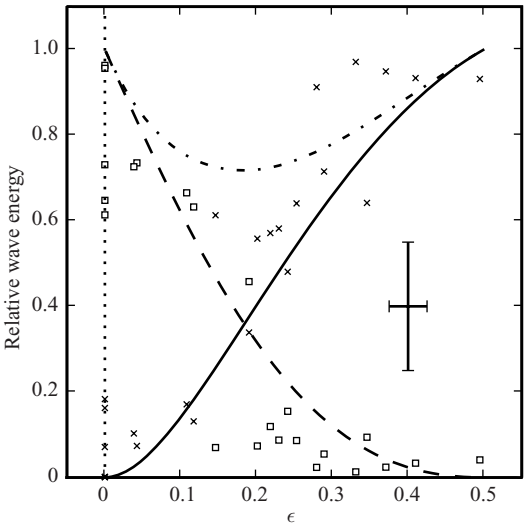


FIGURE 9. Normalized energy of mode-1 (solid line) and mode-2 (dashed line) components versus $\epsilon$ for (3.3). The dotted-dashed line shows the sum of mode-1 and mode-2 energies. The cross-over point where the mode-1 energy begins to exceed the mode-2 energy occurs at $\epsilon \simeq 0.18$ and the minimum energy captured by the mode-1 and mode-2 components is 0.72. The data points show the relative energy in the mode-1 component (crosses) and in the mode-2 component (squares) as computed from a range of experiments. Typical error bars of the experimental data are indicated.

with figure 7. The internal waves no longer couple to the head of the current but propagate well in front of it. Simultaneously, upon reflection from the endwall of the lock, the return flow excites internal waves that catch up with the intrusion head, pinching it into a wedge shape and causing the intrusion to stop propagating.

The increase in phase speed is due to a change in the structure of the internal waves. There is a transition between internal waves with a mode-2 vertical structure for small values of $\epsilon$ to a mode-1 vertical structure for larger values of $\epsilon$. In general, the waves observed in our experiments are a superposition of different wave modes. Nevertheless, the dominant behaviour is characterized by a superposition of mode-1 and mode-2 waves. A long mode-$n$ internal wave has a phase speed given by $c = NH/n\pi$. These phase speeds for long mode-1 and mode-2 waves are superimposed in figure 8 as solid lines.

To understand the transition from mode-2 to mode-1, consider an idealized internal wave with normalized vertical displacement given by

$$f(z) = \begin{cases} \sin\left(\frac{\pi(z/H - 1/2 + \epsilon)}{1/2 + \epsilon}\right) & \frac{z}{H} \geqslant \frac{1}{2} - \epsilon \\ -\frac{1/2 - \epsilon}{1/2 + \epsilon} \sin\left(\frac{/H}{1/2 - \epsilon}\right) & \frac{z}{H} \leqslant \frac{1}{2} - \epsilon \end{cases} \tag{3.3}$$

This function was chosen as an approximation to the actual vertical displacements of the dye lines. At the matching point, $z/H = 1/2 - \epsilon$, this function is continuous and has a continuous first derivative. Further justification or this choice of function is given below.

A discrete sine transform was used to compute the amount of relative energy in the first and second modes of the vertical displacements of dye lines. These energies are plotted against $\epsilon$ in figure 9. Also plotted is a Fourier sine decomposition of

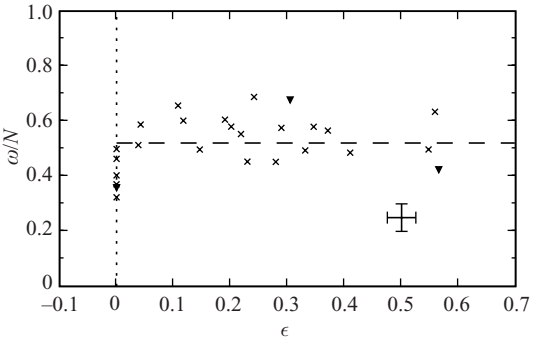


FIGURE 10. Frequency of the internal wave normalized by the buoyancy frequency in experiments with $\ell = 18.5\,\text{cm}$ and $H = 30\,\text{cm}$ (crosses) and $H = 15\,\text{cm}$ (upside-down triangles). The dashed line shows the mean frequency. Typical error bars are indicated.

the first two coefficients (squared) ($b_1^2$ and $b_2^2$) of (3.3). The typical error bars for the relative wave energy, shown to the right, reflect the coarse determination of the wave amplitudes from a discrete set of dye lines. Despite these errors, the analytical model and the experimental data confirm that for low values of $\epsilon$, the internal wave is primarily mode-2, as indicated by the fact that the squares (representing the fraction of energy in mode-2 waves) lie above the crosses (representing the fraction of energy in mode-1 waves). For $\epsilon > 0.18$, energy in mode-1 exceeds that in mode-2 waves, and correspondingly the crosses lie above the squares. The analytical model suggests that the mode-1 and mode-2 components account for at least 70 % of the total internal wave energy.

Thus the intrusion exists in one of three regimes depending upon the value of $\epsilon$. For $\epsilon \simeq 0$, the advance of the intrusion is supercritical to the mode-2 internal waves that are dominantly excited, for $0.18 \lesssim \epsilon \lesssim 0.6$ the intrusion and bottom-propagating gravity currents are subcritical to mode-1 internal waves that are dominantly excited, and for $\epsilon \gtrsim 0.6$ the bottom-propagating gravity currents are supercritical to the mode-1 waves that are dominantly excited.

Figure 10 shows that the frequency $\omega$ of these waves normalized by the buoyancy frequency is independent of $\epsilon$ with $\epsilon \neq 0$ and has a mean value of 0.52 and a standard deviation of 0.10 over all experiments. Although one might expect that the collapse of the lock fluid would generate a spectrum of frequencies, the waves themselves are excited in a narrow frequency band. This frequency selection has been observed in a variety of experiments and simulations in which waves were generated by grid-generated turbulence (Dohan & Sutherland 2002, 2003), turbulence resulting from flow over rough topography (Aguilar & Sutherland 2006), and from an intrusion at the interface of a uniform density fluid and a uniformly stratified fluid (Flynn & Sutherland 2004).

Because $\omega$ is comparable to $N$, the waves cannot be treated as long. The phase speed of a mode-$n$ internal wave of frequency $\omega$ is given by $c = (H/n\pi)\sqrt{N^2 - \omega^2}$. Since we found on average $\omega = 0.52N$, we can compute the speed of a typical mode-1 and mode-2 waves. These speeds are plotted as dashed lines in figure 8. These phase speeds underestimate the phase speeds observed in our experiments. The fact that the observed phase speeds are larger than what linear theory predicts indicates the waves are nonlinear.

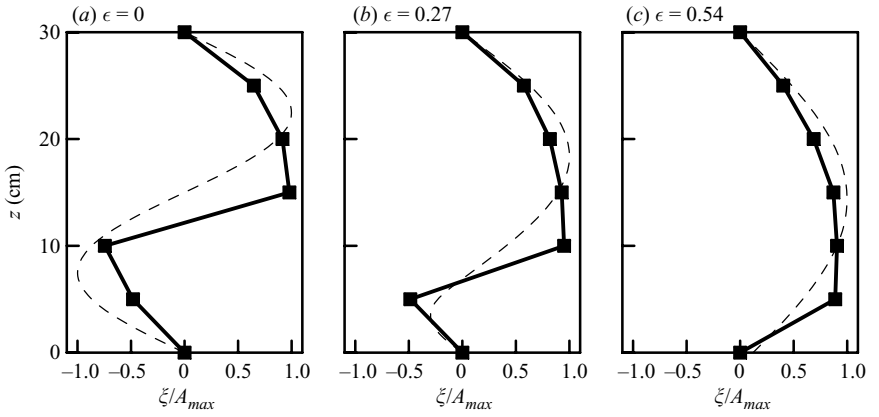


FIGURE 11. Normalized maximum vertical displacement of dye lines as function of height taken at $x = 60$ cm and computed over first wave period. The dotted lines show (3.3) plotted for the corresponding value of $\epsilon$ with (*a*) $\epsilon = 0$, (*b*) $\epsilon = 0.27$ and (*c*) $\epsilon = 0.54$.

Figure 11 shows vertical profiles of the maximum vertical displacement of the ambient measured in three experiments from vertical time series examining the displacement of five dye lines at $x = 60$ cm. This distance, a little more than two lock lengths from the gate, is chosen to be sufficiently close to the lock that reflecting waves from the lock-end of the tank do not interact with the intrusion head as it passes this position. The dashed lines in the figure show amplitude profiles using (3.3) overlaid on measurements taken from three sample experiments. The three profiles, which correspond to the experiments with snapshots shown in figures 4–6, clearly reveal displacements with a mode-2 shape if $\epsilon = 0$ (figure 11*a*), a mixed mode-1 and mode-2 shape if $\epsilon = 0.27$ (figure 11*b*), and a mode-1 shape if $\epsilon = 0.54$ (figure 11*c*).

From the amplitude, frequency and vertical mode structure of the waves, we estimate the energy associated with waves in the ambient during the slumping phase of the intrusion. Defining the vertical displacement amplitude $A_\xi$ to be the largest displacement of the set of the five dye lines, the energy density per unit mass is given by

$$\langle E_{wave} \rangle = \frac{1}{2} N^2 {A_\xi}^2. \tag{3.4}$$

The energy per unit tank width associated with the ambient is then estimated by multiplying the energy density by the area

$$\mathscr{A}_{wave} = \begin{cases} (1 + 2|\epsilon|)\ell H & |\epsilon| < 1/2 \\ 2\ell H & |\epsilon| \geqslant 1/2. \end{cases} \tag{3.5}$$

Here the horizontal length scale is assumed to increase in proportion to $\epsilon$ as the waves evolve from having a mode-2 to a mode-1 structure. This is consistent with the observation that the frequency is fixed but the vertical scale doubles as $\epsilon$ increases from 0 to 1/2.

The resulting energy is compared with the available potential energy per unit width of the fluid in the tank before the gate is extracted. This is calculated as the difference between the potential energy of the initial state and the final state that would occur

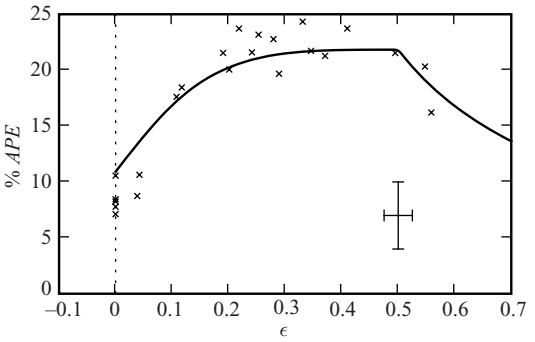


FIGURE 12. Total energy associated with internal waves, shown as a fraction of the initial total APE of the system and plotted versus $\epsilon$. The solid line shows an empirically determined curve using (3.4), (3.5) and (3.9) which is fit to the data using $\alpha = 0.18$ in (3.10). Typical error bars are indicated.

in the absence of mixing

$$APE_0 = \int_0^L \int_0^H g\left(\rho_{initial}(x,z) - \rho_{final}(z)\right) z \, \mathrm{d}z \, \mathrm{d}x. \tag{3.6}$$

In the initial configuration, homogeneous fluid of density $\rho_\ell$ resides in a lock of length $\ell$ beside the uniformly stratified ambient of length $L-\ell$, as shown in figure 1. Explicitly, the density structure is given by

$$\rho_{initial}(x,z) = \begin{cases} \rho_\ell & 0 < x < \ell \\ \rho_B + (\rho_T - \rho_B)\frac{z}{H} & \ell < x < L. \end{cases} \tag{3.7}$$

Assuming no mixing occurs, the final state is that of a piecewise-uniform stratified fluid with a horizontal slab of fluid of density $\rho_\ell$ occupying the full length $L$ of the tank about the neutrally buoyant depth of the ambient before the experiment begins (see figure 4*d*). From conservation of mass of the lock- and ambient-fluid, this final density profile is given by

$$\rho_{final}(z) = \begin{cases} \rho_\ell + (\rho_T - \rho_\ell)\frac{z-h_0}{H-h_0} & h_0 < z < H \\ \rho_\ell & h_1 < z < h_0 \\ \rho_B + (\rho_\ell - \rho_B)\frac{z}{h_1} & 0 < z < h_1. \end{cases} \tag{3.8}$$

If $\rho_\ell < \rho_B$, then

$$h_1 = \frac{\rho_\ell - \rho_B}{\rho_T - \rho_B} H \frac{L-\ell}{L} \text{ and } h_0 = h_1 + H\frac{\ell}{L}.$$

Otherwise, if $\rho_\ell > \rho_B$, then $h_1 = 0$ and $h_0 = H\ell/L$. The available potential energy (APE) per unit width is thus given by

$$APE_0 = \frac{1}{24}\rho_0 \left(1 - \frac{\ell}{L}\right) \ell H^3 N^2 \begin{cases} 12\epsilon^2 + 1 & |\epsilon| < 1/2 \\ 12|\epsilon| - 2 & |\epsilon| > 1/2, \end{cases} \tag{3.9}$$

which increases with the absolute value of $\epsilon$ and with the strength of the stratification.

Using (3.9) to normalize the energy associated with waves given by (3.4) and (3.5), we compute the relative percentage of energy and plot this against $\epsilon$ in figure 12. The internal waves generated by the release of the lock fluid accounted for between 7 % and 22 % of the APE in the system over 25 experiments where the vertical displacements were measured. This is smaller than the 36 % of energy determined

by Ungarish & Huppert (2006) for the case $\epsilon = 1/2$ in part because we make a conservative estimate of the wave energy based upon the one wavelength of the disturbance determined by the lock length and the wave-mode, the latter which depends upon $\epsilon$. The relative energy is larger between $\epsilon = 0.1$ and 0.5, corresponding to the cases in which the intrusion stopped before reaching the end of the tank. This analysis demonstrates that a significant enough amount of the APE goes into internal waves and this energy transfer, as a result, significantly influences the dynamics of an intrusion not only at long times but also during the initial stages of its evolution.

### 3.3. *Wave amplitudes and energy*

To illustrate this impact, we assume the depth-relative amplitude of the waves increases linearly with $\epsilon$ until this parameter exceeds 1/2. Thereafter the amplitude is assumed to be constant. By symmetry, we expect the relative amplitude to double as $\epsilon$ increases from 0 to 1/2. Therefore, we have

$$A_\xi/H = \begin{cases} \alpha(1/2 + |\epsilon|) & |\epsilon| \leqslant 1/2 \\ \alpha & |\epsilon| > 1/2. \end{cases} \tag{3.10}$$

Using this formula, we compute the associated energy of the waves over a volume given by (3.5) and empirically determine the value of $\alpha$ that fits the observed data. Explicitly, we find $\alpha = 0.18 \pm 0.01$. This implies, in particular, that intrusions with $\epsilon \simeq 0.5$ excite internal waves whose amplitudes are almost one-fifth the tank depth.

The corresponding energy normalized by the initial APE of the system is plotted as the solid line in figure 12. Note that the relative energy decreases for $\epsilon > 1/2$ because the energy associated with waves generated by bottom-propagating currents is constant whereas the APE of the system increases with increasing density of the lock fluid.

As the waves change from mode-2 to mode-1, their amplitude and wavelength doubles and so their associated APE increases by a factor of 8. Meanwhile, the APE associated with the lock fluid given by (3.9) increases by a factor 4 as $\epsilon$ changes from 0 to 1/2. Therefore, as expected from symmetry. the percentage change in relative APE is twice as large for mode-1 waves with $\epsilon = 1/2$ as for mode-2 waves with $\epsilon = 0$.

### 3.4. *Intrusion propagation distance*

A universal feature of our experiments is that the intrusions started off at an initially constant speed after a brief acceleration phase. In some cases the intrusion propagated to the end of the tank where it stopped due to the rigid vertical boundary. This occurred either in experiments with $\epsilon \sim 0$ or $\epsilon \gg 1/2$. Otherwise, due to interactions with internal gravity waves, the intrusion stopped abruptly midway along the tank.

Figure 13 shows the relative distance the intrusion travelled in units of lock lengths before this stopping first occurred.

Such an interaction between internal waves and subcritical bottom-propagating gravity currents was also observed by Maxworthy *et al.* (2002). An estimate of the distance over which the waves interact strongly with the current head was provided by Ungarish & Huppert (2004), who claimed the internal waves were locked with the head over the first two wavelengths of motion. Thereafter the waves 'unlocked from the head and move forward relative to the current until the crest reaches the nose (and thus slows it down)'. Our intrusion experiments demonstrate a different interaction mechanism. As shown, for example, in Figure 2(*a*), we find the waves are not locked with the head but advance at constant speed towards the intrusion head after reflecting from the lock-end of the tank. The current does not slow down after

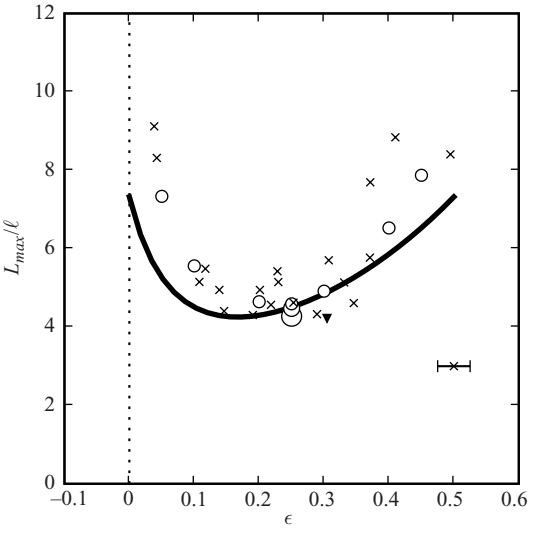


FIGURE 13. Maximum distance travelled by intrusion in experiments with $\ell = 18.5\,\text{cm}$ and $H = 30\,\text{cm}$ (crosses) and $H = 15\,\text{cm}$ (upside-down triangles). The results of numerical simulations are shown by open circles. For these $H = 30\,\text{cm}$. Small, medium and large circles represent the intrusion distances found in simulations with $\ell = 18.6$, 40 and 80 cm, respectively. Typical errors in estimating $\epsilon$ in experiments are indicated towards the bottom right-hand side of the plot. Values are plotted only for those experiments in which the intrusion did not interact with the far end of the tank before being stopped by internal waves catching up to the intrusion head from the lock-end of the tank.

interacting, but stops abruptly. Stopping occurs if the intrusion speed is slower than the internal wave speed.

The speed of both waves and intrusions depends upon the value of $\epsilon$. If $\epsilon \sim 0$ the intrusion speed is comparable to the mode-2 internal wave speed. If $\epsilon \gg 1/2$, the bottom-propagating gravity current propagates at speeds comparable to or faster than the mode-1 internal wave speed. In both circumstances the intrusion is supercritical and so waves reflecting from the lock-end of the tank do not catch up with the intrusion head.

At intermediate values of $\epsilon$, the return flow into the lock excites internal waves that reflect off the lock-end of the tank and then propagate towards the intrusion head at a faster speed than the intrusion itself: the intrusion is subcritical. The advance of the intrusion stops when the waves catch up with the head. This occurs on a time scale which, for fixed $N$ and $H$, depends upon the mode number (depending upon $\epsilon$) and the lock length.

We estimate the stopping distance of intrusions from the time taken for internal waves generated in the return flow to reflect off the lock-wall of the tank and then catch up to the intrusion head. We crudely estimate the speed of these waves to be given by

$$c = \frac{NH}{\pi}(1/2 + |\epsilon|) \quad |\epsilon| \leqslant 1/2. \tag{3.11}$$

This corresponds to a linear increase in the phase speed from that of mode-2 to mode-1 waves as $\epsilon$ increases from 0 to 0.5. The relative distance from the gate that a subcritical intrusion moving at speed $U_{gc}$ travels before internal waves at speed

$c > U_{gc}$ catch up to it is

$$\frac{L_{max}}{\ell} = \frac{2U_{gc}}{c - U_{gc}}. \tag{3.12}$$

Using (3.1) and (3.11) gives the solid curve plotted in figure 13. This estimate agrees well with the observed stopping distance of the intrusion.

## 4. Numerical simulations

### 4.1. *Description of code*

Two-dimensional numerical simulations were performed to compare with the experimental results, as well as to obtain additional insight into the energy balance of the flow. The Navier–Stokes equations in vorticity streamfunction formulation are employed for the numerical simulation. The vorticity streamfunction formulation of the non-dimensional governing equations with the Boussinesq assumption can be written as

$$\frac{\partial^2 \psi}{\partial x_i \partial x_i} = -\omega, \tag{4.1}$$

$$\frac{\partial \omega}{\partial t} + u_i \frac{\partial \omega}{\partial x_i} = \frac{1}{Re} \frac{\partial^2 \omega}{\partial x_i \partial x_i} - \frac{\partial \rho}{\partial x_1}, \tag{4.2}$$

$$\frac{\partial \rho}{\partial t} + \frac{\partial (\rho u_i)}{\partial x_i} = \frac{1}{ReSc} \frac{\partial^2 \rho}{\partial x_i \partial x_i}. \tag{4.3}$$

The equations are non-dimensionalized using the tank height $H$ as the length scale and the inverse buoyancy frequency $N^{-1}$ as the time scale. The two governing dimensionless parameters in (4.1)–(4.3) are the Reynolds number $Re$, and the Schmidt number $Sc$, which are defined as $Re = NH^2/\nu$ and $Sc = \nu/\kappa$, where $\nu$ is kinematic viscosity and $\kappa$ is the coefficient of molecular diffusivity. Numerical simulations were performed with $Re = 20\,000$, comparable to values in experiments, and sufficiently large that viscous effects do not play an important role. The Schmidt number was set to be unity, rather than the experimental value of 1000. Although smaller than the corresponding values in laboratory experiments, this was large enough that molecular dissipative effects negligibly affected the intrusion evolution while not being so large that the code became numerically unstable.

The domain is rectangular with the same aspect ratio as the fluid in the laboratory experiments. The grid size of $N_x = 2049$ and $N_y = 240$ is used for all the simulations. The lock length $\ell$ likewise was set to mimic the experiments. Initially the lock fluid was assigned a density $\rho_\ell$. At the gate location we assume the vertical interface between the lock and ambient has a thickness of $O(0.01)$ over which the density smoothly changes from its lock value to the ambient value. No-slip boundary conditions are employed at the top and bottom walls, while slip is allowed at the left and right walls. The simulations employ equidistant grids in the rectangular computational domain. Spectral Galerkin methods are used in representing the streamwise dependence of the streamfunction and the vorticity fields as explained in Härtel *et al.* (2000). Vertical derivatives are approximated with sixth order in the centre and third at walls, on the basis of the compact finite difference stencils described by Lele (1992). A third-order Runge–Kutta time integration scheme is employed to evolve governing equations in time. The computational procedure used is very similar to that described in Härtel *et al.* (2000). Further details of the validation of the code are provided in Härtel *et al.* (2000).

The non-dimensional energy equation derived from the governing equations can be written as (Necker *et al.* 2005, cf.)

$$\frac{\mathrm{d}}{\mathrm{d}t}(E_k + E_p) = -\frac{2}{Re}\int_\Omega s_{ij}s_{ij}\,\mathrm{d}V, \tag{4.4}$$

where $s_{ij}$ denotes the rate of strain tensor, $E_k(t)$ is the non-dimensional kinetic energy and $E_p(t)$ is the potential energy of the flow. In non-dimensional form they can be expressed as

$$s_{ij} = \frac{1}{2}\left(\frac{\partial u_i}{\partial x_j} + \frac{\partial u_j}{\partial x_i}\right), \tag{4.5}$$

$$E_k = \frac{1}{2}\int_\Omega u_i u_i\,\mathrm{d}V, \tag{4.6}$$

$$E_p = \int_\Omega \rho z\,\mathrm{d}V \tag{4.7}$$

Equation (4.4) shows that during the flow the total energy, i.e. the sum of kinetic energy, potential energy and dissipated energy remains constant. We can numerically calculate the kinetic energy, potential energy and dissipation energy as functions of time as the flow evolves.

In particular, we examine the evolution of the APE over time. The initial APE is defined, as in (3.6), to be the difference in potential energy between the state when the lock fluid is mixed and still behind the gate and the minimum-energy state, given by (3.8), in which this fluid lies in a horizontal slab at its neutral density level. At later times, the total APE is computed from the corresponding integral with $\rho_{initial}$ replaced by the instantaneous density $\rho(x, z, t)$. In practice a threshold is set so that fluid associated with the intrusion has a density change from the initial lock fluid which is no more than 1 % of the maximum absolute value of the density difference between the density of the initial lock fluid and the ambient.

In order to assess how the energy associated with the intrusion is transferred to the stratified ambient, we further partition the domain of integration into two parts, one associated with the area occupied by fluid having the same density as the lock fluid and the remaining area being that associated with the perturbed ambient. The resulting integrals over each area we refer to as the 'intrusion APE' and the 'ambient APE', respectively. The sum of the two quantities is the 'total APE', in the normal sense of APE.

### 4.2. *Results*

Snapshots from three simulations having parameters similar to the experiments highlighted in figures 4–6 are shown in figure 14. These are plots of the total density field. The greyscales are constructed so that grey contours are plotted at the corresponding level of the dye lines in the laboratory experiments and black contours are drawn where the density is comparable to the initial lock fluid density.

The simulations are qualitatively and quantitatively similar to the laboratory experiments. A symmetric intrusion, with $\epsilon = 0$, propagates to the end of the domain and excites a mode-2 disturbance that surrounds the intrusion head but which does not propagate ahead of the intrusion. If symmetry is broken by increasing $\epsilon$, a complex internal wave field is excited in the ambient which moves well ahead of the intrusion head and an internal wave reflecting from the lock-end of the tank catches up to the intrusion and halts its advance. If $\epsilon = 0.5$, the intrusion excites a mode-1 wave that propagates ahead of the intrusion. For still large $\epsilon$

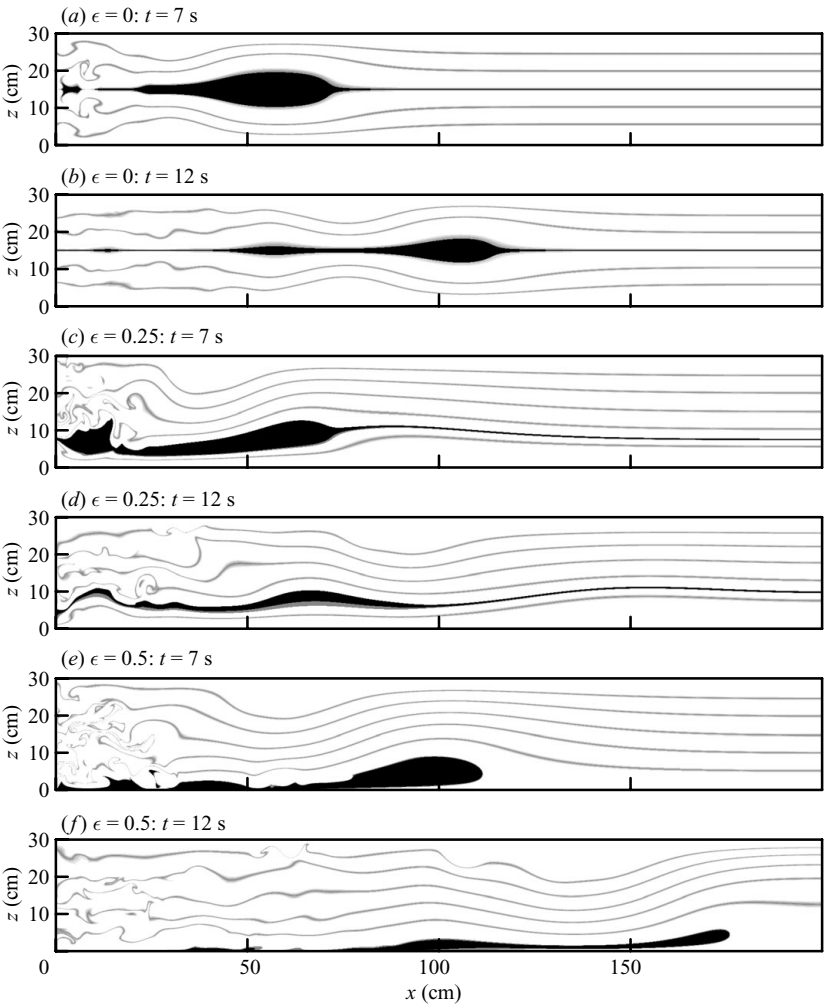


FIGURE 14. Snapshots from three numerical simulations with $\epsilon = 0$ at (*a*) $t = 7$ s and (*b*) $t = 12$ s, with $\epsilon = 0.25$ at (*c*) $t = 7$ s and (*d*) $t = 12$ s and with $\epsilon = 0.50$ at (*e*) $t = 7$ s and (*f*) $t = 12$ s.

(not shown) the bottom-propagating gravity current is supercritical and internal waves reflecting from the lock-end of the tank do not catch up with the intrusion head.

In the laboratory experiments, the gate is extracted over a small, but finite time whereas the release of fluid from the lock is instantaneous in the simulations. The fact that the simulated intrusion and wave field have similar structure to the experiments indicates that the asymmetry resulting from extracting the gate in experiments does not significantly affect the flow evolution.

For example, figure 15(*a*) shows the position of the intrusion head as it advances in time in three simulations with $\epsilon = 0$, 0.31 and 0.68. Consistent with the experiments, the plots show that the currents travel at constant speed for up to 10 lock lengths with the speed increasing as $\epsilon$ increases. In the case with $\epsilon = 0.31$ the current stops propagating approximately three lock lengths from the gate as a consequence of interactions with internal waves.

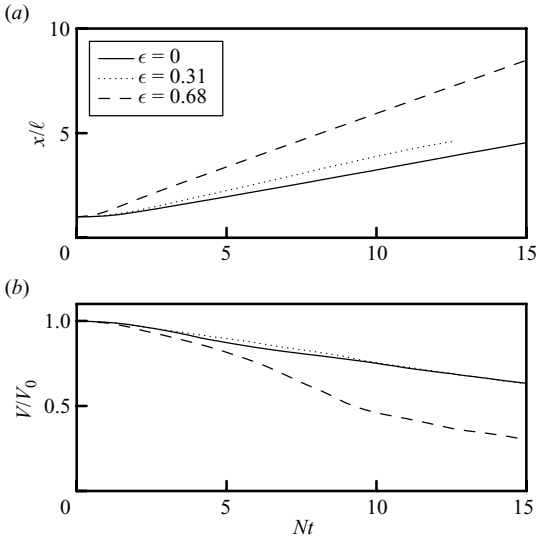


FIGURE 15. (*a*) Location of intrusion head and (*b*) volume of the intrusion as it evolves over time. Results are shown for three simulations with the same dynamical parameters as the experiments shown in figures 4–6, with corresponding lines indicated in the legend inset in (*a*).

The simulated non-dimensional speeds are $U_{gc}/NH = 0.133$, 0.162 and 0.32 for $\epsilon = 0$, 0.31 and 0.68, respectively. Comparing these with the speeds observed in experiments, as shown in figure 7, we find good agreement within the scatter of data.

To examine the effect of lock length upon the evolution of the intrusion, we have performed simulations of intrusions released from longer locks in longer horizontal domains. Figure 16 shows the results of three simulations in which $\epsilon = 0.25$ and the lock length has values of $\ell = 18.6$, 40 and 80 cm. In all three cases $H = 30$ cm and $N = 1\,\mathrm{s}^{-1}$. When the horizontal is rescaled by $x/\ell$ and time is rescaled by $Nt$, we see that waves advancing from the lock-end of the tank catch up with the intrusion head at approximately the same rescaled time and position. The (un-rescaled) horizontal wavelength of internal waves is the same in all three cases, confirming that the horizontal wavelength is set by the tank depth, not the lock length. Also, in each case the intrusion speed is constant until it stops. The stopping distance, plotted by the small, medium and large open circles in figure 13, shows the rescaled distance is the same in all three simulations.

Likewise in simulations with $\epsilon = 0$ and $\epsilon = 0.5$, we observe that the intrusion propagates at constant speed which is comparable to the mode-2 and mode-1 internal wave speeds, respectively. In these cases the intrusion does not stop but the lock fluid is carried by the waves similar to the transport of fluid by closed-core solitary waves (e.g. see Sutherland & Nault 2007).

The volume of the three intrusions shown in figure 14 is examined in figure 15(*b*). This is calculated as the volume of fluid having the same density as the fluid initially in the lock. As expected, the volume decreases in all three cases due to mixing. In the two intrusion cases with $\epsilon = 0$ and 0.31, the volume decreases at nearly the same rate over time, whereas the volume of the bottom-propagating gravity current decreases much more rapidly. Presumably this is because the faster moving current exhibits more vigorous mixing.

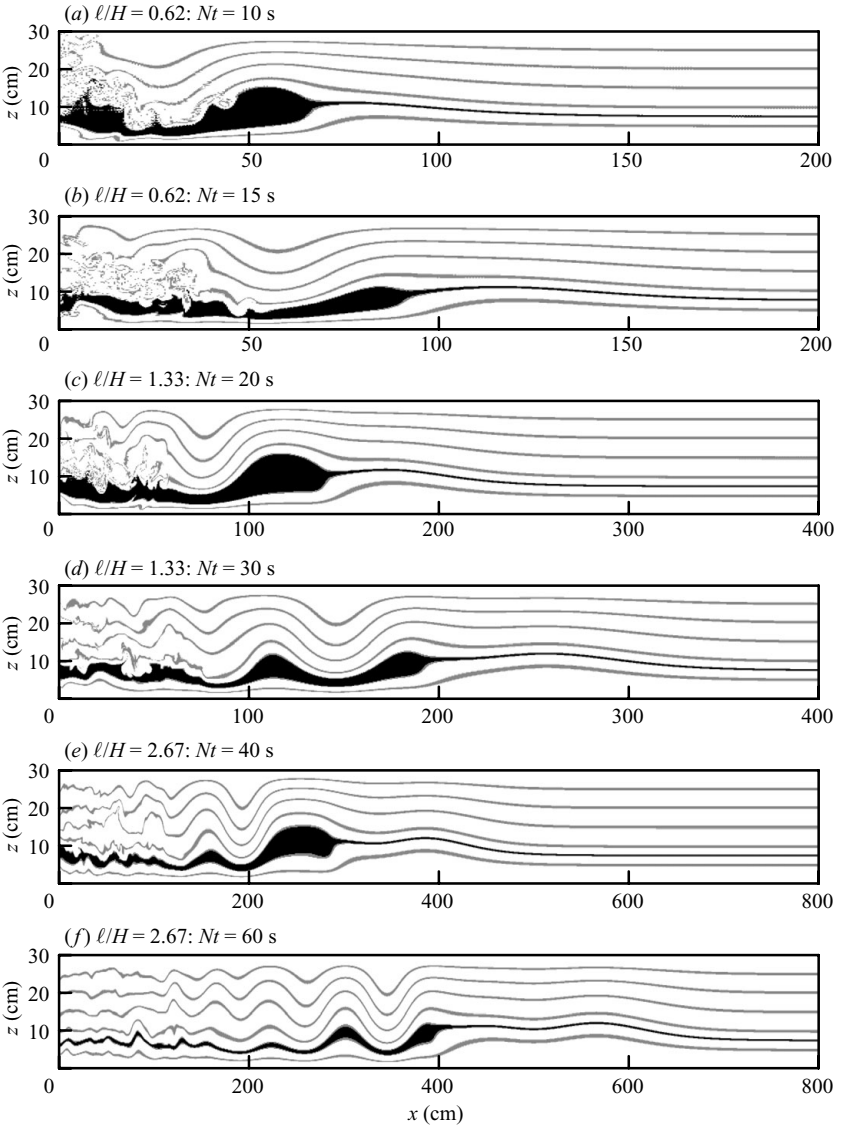


FIGURE 16. Same as in figure 14, but showing snapshots at two times from each of three numerical simulations with $\epsilon = 0.25$ and (*a*), (*b*) $\ell = 18.6$, (*c*), (*d*) $\ell = 40$, and (*e*), (*f*) $\ell = 80$ cm. In all three cases $H = 30$ cm and $N = 1\,\mathrm{s}^{-1}$. In simulations with larger $\ell$, the horizontal extent of the domain is larger and the time at which the snapshot is shown is larger.

It is encouraging to note that the position and structure of the intrusions in the three simulations agree well with the corresponding laboratory experiments. Thus the neglect of fully three-dimensional mixing in the simulations does not significantly effect the evolution of the intrusions and the wave fields they produce.

Figure 17 shows the available potential and kinetic energies associated with the intrusion and ambient as the system evolves over time. The graphs are normalized by the initial total APE, given by (3.9). Before release the APE associated with the intrusion is positive and that with the ambient is negative. As the intrusion collapses

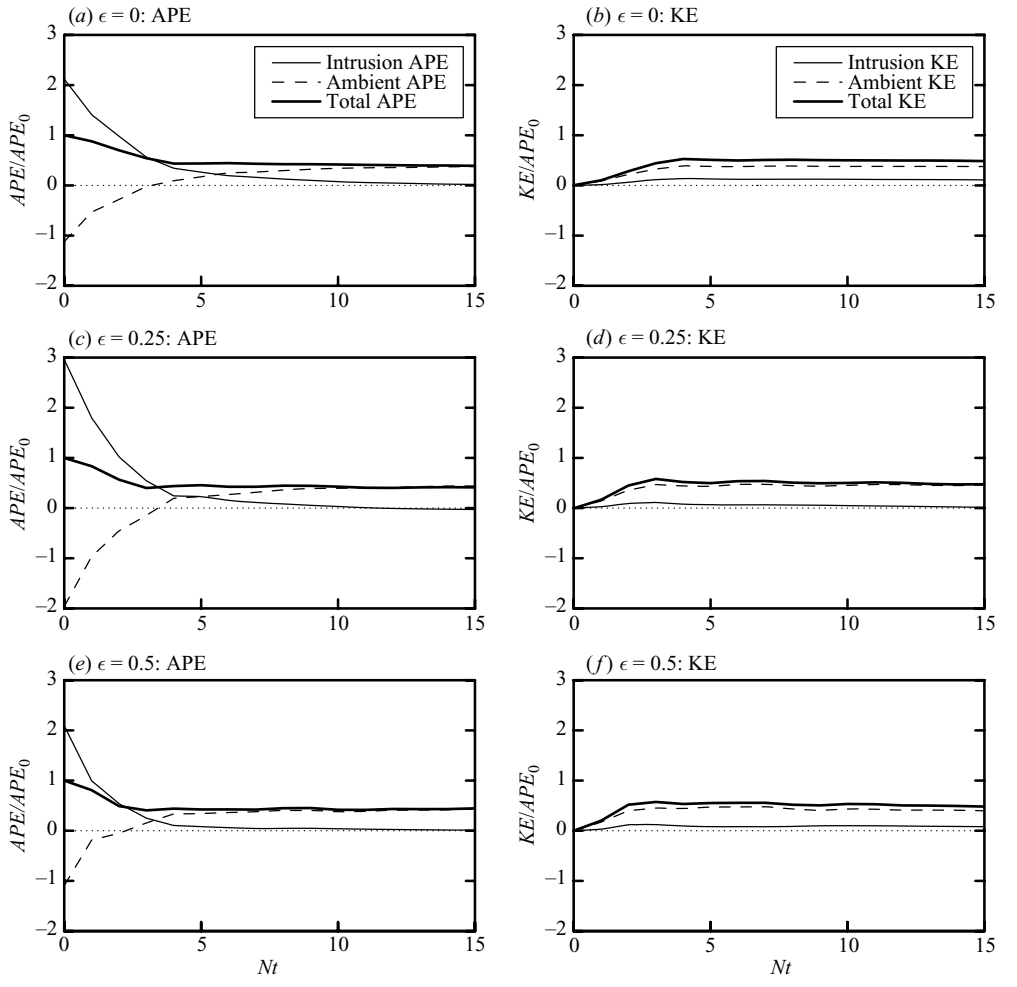


FIGURE 17. Available potential energy (left panel) and kinetic energy (right panel) associated with the intrusion (thin solid line) and ambient (dashed line). The total energies are plotted as the thick solid line. These are computed in three simulations with $(a,b)$ $\epsilon = 0$, $(c,d)$ $\epsilon = 0.25$ and $(e,f)$ $\epsilon = 0.5$.

it imparts APE to the ambient as well as converting it in part to kinetic energy and losing it to dissipation. Values of the kinetic and available potential energies of the intrusion and ambient at different times are listed in table 1.

In simulations with increasing $\epsilon$, a qualitative change in the evolution of each component of the APE is observed. This is illustrated in figure 17. In all three simulations, the initial APE associated with the lock fluid is rapidly converted into kinetic energy and the APE of the ambient, the two being nearly in equipartition. The time taken for energy to transfer to the ambient is longest for the case with $\epsilon = 0$. The ambient has as much APE as the intrusion at time $Nt = 5.5$ and after non-dimensional time $Nt = 15$, only 4 % of the APE is associated with the intrusion. Although the APE and kinetic energy of the ambient are close to equipartition after $Nt = 10$, the kinetic energy of the intrusion is 30 % of the kinetic energy of the ambient.

| | *Nt* | 3 | 9 | 15 |
|---|---|---|---|---|
| $\epsilon = 0$ | Intr. APE | 0.564 | 0.101 | 0.021 |
| | Amb. APE | −0.021 | 0.322 | 0.377 |
| | Intr. KE | 0.116 | 0.125 | 0.111 |
| | Amb. KE | 0.327 | 0.380 | 0.377 |
| $\epsilon = 0.25$ | Intr. APE | 0.544 | 0.053 | −0.028 |
| | Amb. APE | −0.144 | 0.391 | 0.440 |
| | Intr. KE | 0.112 | 0.058 | 0.016 |
| | Amb. KE | 0.469 | 0.437 | 0.459 |
| $\epsilon = 0.5$ | Intr. APE | 0.251 | 0.048 | 0.011 |
| | Amb. APE | 0.155 | 0.404 | 0.432 |
| | Intr. KE | 0.122 | 0.099 | 0.081 |
| | Amb. KE | 0.452 | 0.406 | 0.397 |

TABLE 1. Intrusion and ambient available potential energy (APE) and kinetic energy (KE) given as a fraction of the total initial APE of the system. Values are extracted from three numerical simulations with $\epsilon = 0$, 0.25 and 0.5 and are given at times $Nt = 3$, 9 and 15. The same quantities are plotted for times between $Nt = 0$ and 15 in figure 17.

In the case with $\epsilon = 0.25$, the APE of the lock fluid transfers rapidly to the ambient and by time $Nt = 15$, almost all the energy is associated with the ambient fluid, the kinetic and available potential energies being in equipartition.

Although the transfer of energy from intrusion to ambient energy is faster still in the case $\epsilon = 0.5$, as in the case with $\epsilon = 0$, a significant fraction (20 %) of energy remains associated with the intrusion by time $Nt = 15$.

These observations lie in contrast with the shallow-water theory results of Ungarish & Huppert (2006). They showed that for subcritical bottom-propagating gravity currents, the interaction between waves and the current head could not be detected by analysis of the energetics of the system in the case $S = 0.72$ ($\epsilon = 0.89$). In the case $S = 1$ ($\epsilon = 1/2$), they found that, in comparison with numerical simulations, shallow-water theory significantly underpredicted the total mechanical energy of the current shortly after being released from the lock. Thus shallow-water theory, while performing well for bottom-propagating currents in weakly stratified ambients, does not well capture the observed energetics of subcritical currents in strongly stratified ambients and, by extension, has questionable applicability to intrusive gravity currents.

## 5. Discussion and conclusions

Experiments and numerical simulations have investigated intrusions and their interactions with internal waves in a uniformly stratified ambient. That the two-dimensional simulations capture the observed structure and speed of the intrusions indicates that their macroscopic dynamics can be well described by a two-dimensional model. The speed of the intrusion was found to match the prediction of Bolster *et al.* (2008) in circumstances with $\epsilon < 0.5$. For $\epsilon > 0.5$, the theoretical prediction of Ungarish & Huppert (2002) and the empirical prediction of Maxworthy *et al.* (2002) is close to the observed speed of bottom-propagating gravity currents, though theory moderately underpredicts the speed.

It is well-established that a gravity current in a uniform-density ambient propagates 6–10 lock lengths before entering the 'self-similar' phase in which the current decelerates. This occurs because the finite volume of lock fluid requires the head-height to decrease and, consequently, the horizontal pressure gradient force driving the current decreases. Our results show this does not occur for intrusions released into a uniformly stratified ambient from a high aspect-ratio lock. Internal waves interacting with the intrusion head dominate the long-time evolution of the intrusion. In symmetric cases, the waves propagate at the same speed as the intrusion and carry the lock fluid at constant speed well past 10 lock lengths, even though the vertical extent of the head decreases substantially. In asymmetric cases, waves that reflect from the lock-end of the tank catch up with the head and halt its advance. Thereafter, the lock fluid slowly undulates forward driven dominantly by the wave field and not by horizontal pressure gradients established through horizontal density changes between the intrusion and ambient.

The distance travelled by the intrusion before stopping is related to the wave speed of the internal waves generated. Intrusions travelling near the mid-depth of the tank excite mode-2 waves. In the limit of an intrusion becoming a gravity current, more mode-1-like waves are produced. Mode-1 waves travel faster than mode-2 waves and faster than the intrusion for intermediate values of $\epsilon$. The mode-1 waves, which reflect off the rear wall of the tank and then catch up with the intrusion head, cause the intrusion to stop before hitting the end of the tank. The energy associated with the waves lies between 10 % and 20 % of the initial APE of the lock fluid. This may not be so large as to have a leading-order effect upon the intrusion speed, but it is large enough to affect non-negligibly the consequent evolution of the intrusion in terms of the propagation distance. Energy analyses of intrusions in numerical simulations show that a substantial fraction of the initial APE is transferred to the ambient if $\epsilon$ is sufficiently larger than zero and mode-1 waves are predominately excited. Experimental data were used to derive an empirical formula for the wave energy. This result showed that, for bottom-propagating gravity currents, the energy of waves relative to the initial APE decreases as $\epsilon$ increases. These results are consistent with the observation that internal waves do not strongly influence the consequent motion of the current if $\epsilon$ is large.

In none of the experiments performed did we observe the transition from steady-state to self-similar propagation of the intrusion, as predicted by Ungarish (2005). The symmetric intrusion propagates beyond 10 lock lengths without deceleration. Indeed, Sutherland & Nault (2007) have shown that symmetric intrusions can propagate up to 22 lock-lengths without decelerating as a result of coupling with mode-2 internal waves. The long-time evolution in this case is best described by the propagation of closed core solitary waves in this case. Asymmetric intrusions with $0.18 \lesssim \epsilon < 0.5$ propagate at constant speed until suddenly stopping due to interaction with internal waves.

Some signature of a self-similar phase seemed to occur in experiments by Wu (1969) and Amen & Maxworthy (1980), consistent with shallow-water predictions (Ungarish 2005). So why was the self-similar phase not observed in our experiments? A likely explanation is that those experiments generated symmetric intrusions from the collapse of a mixed region that did not extend over the full depth of the tank, a circumstance that is better described by the approximations of shallow-water theory. Thus it seems in those circumstances that the collapsing mixed fluid did not excite such large amplitude internal waves and that the fluid became sufficiently diluted through

mixing with the ambient that its advance slowed. Clearly more experiments on partial-depth mixed region collapse should be performed to examine this circumstance in more detail.

In order to focus upon the interactions between intrusions and internal waves, our laboratory experiments were confined to the examination of relatively short locks compared to the length of the tank. In longer tanks with longer locks a proportionally smaller volume of the intrusion would mix with the ambient. In these circumstances it may be that asymmetric intrusions would evolve into a self-similar phase before interacting with internal waves reflecting from the lock-end of the tank (Paul F. Linden, private communication 2007). Nonetheless, we have seen that symmetric intrusions (with $\epsilon = 0$) propagate over 10 lock lengths without decelerating all the while with the head-height decreasing. Internal waves locked to the intrusion head, not horizontal density gradients between the intrusion and ambient, are responsible for the transport at constant speed. Likewise, in asymmetric circumstances the intrusion stops due to interactions with internal waves and thereafter the transport of lock fluid is governed primarily by the waves, not horizontal density gradients. In general, the experimental and numerical results show that the long-time evolution of intrusions in uniformly stratified fluid is not necessarily well modelled by a straightforward adaptation of Benjamin's theory that neglects the generation and consequent influence of internal waves upon the flow.

We are grateful to the reviewers and to Paul Linden whose comments helped substantially to improve the paper. The experiments were performed in the Environmental and Industrial Fluid Dynamics Laboratory at the University of Alberta. The authors wish thank Amenda Chow and Tyler Pittman for performing additional experiments. This work was supported by funding from the Canadian Foundation for Climate and Atmospheric Sciences and the Natural Sciences and Engineering Research Council's USRA program.

## REFERENCES

Aguilar, D. A. & Sutherland, B. R. 2006 Internal wave generation from rough topography. *Phys. Fluids* **18**, Art. No. 066603.

Amen, R. & Maxworthy, T. 1980 The gravitational collapse of a mixed region into a linearly stratified solution. *J. Fluid Mech.* **96**, 65–80.

Benjamin, T. B. 1968 Gravity currents and related phenomena. *J. Fluid Mech.* **31**, 209–248.

Birman, V. K., Meiburg, E. & Ungarish, M. 2007 On gravity currents in stratified ambients. *Phys. Fluids* **19**, 086602–1–10. doi:10.1063/1.2756553.

Bolster, D., Hang, A. & Linden, P. F. 2008 The front speed of intrusions into a continuously stratified medium. *J. Fluid Mech.* **594**, 369–377.

Britter, R. E. & Simpson, J. E. 1978 Experiments on the dynamics of a gravity current head. *J. Fluid Mech.* **88**, 223–240.

Britter, R. E. & Simpson, J. E. 1981 A note on the structure of the head of an intrusive gravity current. *J. Fluid Mech.* **112**, 459–466.

Cheong, H., Kuenen, J. J. P. & Linden, P. F. 2006 The front speed of intrusive gravity currents. *J. Fluid Mech.* **552**, 1–11.

Dalziel, S. B. 1992 Decay of rotating turbulence: Some particle tracking experiments. *Appl. Sci. Res.* **49**, 217–244.

Dohan, K. & Sutherland, B. R. 2002 Turbulence time-scales in mixing box experiments. *Exp. Fluids* **33**, 709–719.

Dohan, K. & Sutherland, B. R. 2003 Internal waves generated from a turbulent mixed region. *Phys. Fluids* **15**, 488–498.

Flynn, M. R. & Linden, P. F. 2006 Intrusive gravity currents. *J. Fluid Mech.* **568**, 193–2002.

Flynn, M. R. & Sutherland, B. R. 2004 Intrusive gravity currents and internal wave generation in stratified fluid. *J. Fluid Mech.* **514**, 355–383.

Härtel, C., Meiburg, E. & Necker, F. 2000 Analysis and direct numerical simulation of the flow at a gravity-current head. Part 1. Flow topology and front speed for slip and no-slip boundaries. *J. Fluid Mech.* **418**, 189–212.

Holyer, J. Y. & Huppert, H. E. 1980 Gravity currents entering a two-layer fluid. *J. Fluid. Mech.* **100**, 739–767.

Huppert, H. E. & Simpson, J. E. 1980 The slumping of gravity currents. *J. Fluid Mech.* **99**, 785–799.

Keulegan, G. H. 1957 An experimental study of the motion of saline water from locks into fresh water channels. *Tech. Rep.* 5168. Nat. Bur. Stand. Rept.

Klemp, J. B., Rotunno, R. & Skamarock, W. C. 1994 On the dynamics of gravity currents in a channel. *J. Fluid Mech.* **269**, 169–198.

Lele, S. K. 1992 Compact finite-difference schemes with spectral-like resolution. *J. Comput. Phys.* **103**, 16–42.

Long, R. R. 1953 Some aspects of the flow of stratified fluids. a theoretical investigation. *Tellus* **5**, 42–58.

Long, R. R. 1955 Some aspects of the flow of stratified fluids. III. Continuous density gradients. *Tellus* **7**, 341–357.

Lowe, R. J., Linden, P. F. & Rottman, J. W. 2002 A laboratory study of the velocity structure in an intrusive gravity current. *J. Fluid Mech.* **456**, 33–48.

Manins, P. 1976 Intrusion into a stratified fluid. *J. Fluid Mech.* **74**, 547–560.

Maxworthy, T., Leilich, J., Simpson, J. & Meiburg, E. H. 2002 The propagation of a gravity current in a linearly stratified fluid. *J. Fluid Mech.* **453**, 371–394.

Monaghan, J. J. 2007 Gravity current interaction with interfaces. *Annu. Rev. Fluid Mech.* **39**, 245–261.

Necker, F., Härtel, C., Kleiser, L. & Meiburg, E. 2005 Mixing and dissipation in particle-driven gravity currents. *J. Fluid Mech.* **545**, 339–372.

Oster, G. 1965 Density gradients. *Sci. Am.* **213**, 70.

Rottman, J. W. & Simpson, J. E. 1983 Gravity currents produced by instantaneous releases of a heavy fluid in a rectangular channel. *J. Fluid Mech.* **135**, 95–110.

Schooley, A. & Hughes, B. 1972 An experimental and theoretical study of internal waves generated by the collapse of a two-dimensional mixed region in a density gradient. *J. Fluid Mech.* **51**, 159–175.

Shin, J., Dalziel, S. & Linden, P. 2004 Gravity currents produced by lock exchange. *J. Fluid Mech.* **521**, 1–34.

Silva, I. P. D. D. & Fernando, H. J. S. 1998 Experiments on collapsing turbulent regions in stratified fluids. *J. Fluid Mech.* **358**, 29–60.

Simpson, J. E. 1972 Effects of lower boundary on the head of a gravity current. *J. Fluid Mech.* **53**, 759–768.

Simpson, J. E. 1982 Gravity currents in the laboratory, atmosphere, and ocean. *Annu. Rev. Fluid Mech.* **14**, 213–234.

Simpson, J. E. 1997 *Gravity Currents*, 2nd edn. Cambridge University Press.

Simpson, J. E. & Britter, R. E. 1979 The dynamics of the head of a gravity current advancing over a horizontal surface. *J. Fluid Mech.* **94**, 477–495.

Sutherland, B. R., Chow, A. N. F. & Pittman, T. P. 2007 The collapse of a mixed patch in stratified fluid. *Phys. Fluids* **19**, 116602–1–6. doi:10.1063/1.2814331.

Sutherland, B. R., Kyba, P. J. & Flynn, M. R. 2004 Interfacial gravity currents in two-layer fluids. *J. Fluid Mech.* **514**, 327–353.

Sutherland, B. R. & Nault, J. T. 2007 Intrusive gravity currents propagating along thin and thick interfaces. *J. Fluid Mech.* **586**, 109–118. doi:10.1017/S0022112007007288.

Ungarish, M. 2005 Intrusive gravity currents in a stratified ambient: Shallow-water theory and numerical results. *J. Fluid Mech.* **535**, 287–323.

UNGARISH, M. 2006 On gravity currents in a linearly stratified ambient: a generalization of Benjamin's steady-state propagation results. *J. Fluid Mech.* **548**, 49–68.

UNGARISH, M. & HUPPERT, H. E. 2002 On gravity currents propagating at the base of a stratified fluid. *J. Fluid Mech.* **458**, 283–301.

UNGARISH, M. & HUPPERT, H. E. 2004 On gravity currents propagating at the base of a stratified ambient: effects of geometrical constraints and rotation. *J. Fluid Mech.* **521**, 69–104.

UNGARISH, M. & HUPPERT, H. E. 2006 Energy balances for propagating gravity currents: homogeneous and stratified ambients. *J. Fluid Mech.* **565**, 363–380.

WU, J. 1969 Mixed region collapse with internal wave generation in a density stratified medium. *J. Fluid Mech.* **35**, 531–544.